EVOLUTION OF SHEAR LOCALISATION IN EARTH PRESSURE PROBLEMS OF A RETAINING WALL

JACEK TEJCHMAN

Civil Engineering Department, Gdansk University of Technology,
Narutowicza 11/12, 80-952 Gdansk, Poland
tejchmk@pg.gda.pl

Abstract: The paper deals with numerical investigations of the evolution of shear localisation in granular bodies for earth pressure problems of a retaining wall in conditions of plane strain. The passive and active failure of a retaining wall in sand is discussed. The calculations are carried out with a rigid and very rough retaining wall undergoing horizontal translation, rotation around the top and rotation around the bottom. The behaviour of dry sand is numerically modelled with a finite element method using a hypoplastic constitutive relation within a polar (Cosserat) continuum. The constitutive relation is obtained through extension by polar quantities, *viz.* rotations, curvatures and couple stresses, using the mean grain diameter as a characteristic length. During FE-calculations, the attention is laid on the influence of different wall movements on shear localisation. In addition, the effects of the initial void ratio, distribution of the initial void ratio and mean grain diameter, pressure level and size of the sand body and retaining wall is investigated in the case of a passive wall translation. The FE-results are compared with corresponding experimental results of laboratory model tests.

Keywords: earth pressure, granular material, finite element method, hypoplasticity, polar continuum, retaining wall, shear localisation

1. Introduction

The determination of earth pressures on a retaining wall belongs to the classical problems of soil mechanics. In spite of intense theoretical and experimental research on this problem over more than 200 years, there are still large discrepancies between theoretical solutions and experimental results. The reason is that the deformation field in granular bodies close to the wall is very complex due to shear localisations. These can appear as single, multiple or pattern of shear zones depending mainly on the type of wall movements, wall flexibility and surcharge. Shear zones can be plane or curved. Realistic earth pressures can be only calculated with constitutive models which are able to reproduce the formation of shear zones with a certain thickness and spacing, *i.e.* the constitutive model has to include a characteristic length. There are several approaches to capture shear localisation in granular bodies:

deformation gradient [1–4], viscous [2, 5], non-local [6, 7] and polar ones [7–13]. Using these approaches, FE-results converge to a finite size of shear zones via mesh refinement [1–13], and initial and boundary value problems become mathematically well-posed even when using constitutive laws with softening [3, 8]. Otherwise, FE-results are completely determined by the resolution of the mesh and thus produce unreliable results, *i.e.* the shear zones become narrower upon mesh refinement and computed force-displacement curves change considerably depending on the thickness of the calculated shear zone [7, 10, 14].

Since the geometry of shear localisation depends on mean grain diameter, pressure level, initial density, direction of deformation, grain roughness and grain size distribution [10, 15–19], it is of major importance to use a constitutive model taking into consideration these factors.

In this paper, the evolution of shear localisation is investigated during passive and active earth pressure tests of a retaining wall in sand with a finite element method using a hypoplastic law with polar extensions. The law takes into account the effect of initial density, pressure, deformation direction, mean grain size and grain roughness on shear localisation. The emphasis is placed on the influence of the type of wall movements on shear zones and earth pressures. In addition, the effect of the initial void ratio and its distribution in sand, distribution of the mean grain diameter, pressure level and the specimen size on shear localisation is analysed for the case of a wall translating horizontally away from a granular backfill. Only plane strain case was taken into account.

2. Literature review

Coulomb [20] indicated for the first time the occurrence of shear zones during earth pressure tests. Darwin [21] showed with model tests that the explanation of the behaviour of granular bodies during earth pressure is not possible without taking into account shear localisation and historical effects. Comprehensive experimental studies on earth pressure in sand have been carried out at the Cambridge University [22–30]. The type of the wall movement, wall roughness, wall flexibility, initial density of sand, specimen size, sand type and surcharge were varied. The geometry of shear localisation was recorded on radiographs. Different modes of shear zones have been observed during passive and active earth pressure tests depending strongly on the type of the wall motion, initial density of sand and surcharge. In passive tests with rigid walls rotating about the top, usually one or sometimes two curved shear zones were obtained in sand which started at the wall bottom and propagated towards the free boundary. Multiple curved shear zones of a similar shape were observed during tests with a wall rotating about the bottom. They occurred at the wall top and propagated towards the free boundary. During tests with a translating rigid wall, one nearly circular shear zone starting from the wall bottom, and a fan of secondary nearly radial shear zones beginning at the wall top appeared. In active tests with rigid walls, nearly parallel straight zones or a mesh of intersecting parallel zones close to the wall (wall rotating about the bottom) or a single curved zone (wall rotating about the top) were observed.

Experimental studies of passive earth pressure on a retaining wall in sand were also performed at the Karlsruhe University [31, 32]. During a wall translation, one observed a pattern of shear zones consisting of one major nearly circular shear zone starting at the wall toe, propagating towards the free boundary, and a fan of nearly radial zones from the wall top towards the circular zone, and one (not fully developed) shear zone parallel to the bottom.

Earth pressures on a retaining wall were calculated within a theory of elasticity and plasticity. Assuming that the entire granular body behind a retaining wall behaves elastically and its deformation is small, Boussinesq formulated simple formulas to calculate earth pressures [33]. Within plastic limit states, there are generally two approaches: static and kinematic. In the first approach, which requires an assumption that the material is yielding everywhere behind the wall (according to the Mohr-Coulomb law), one can obtain mathematically closed solutions of pressures for simple cases [33–35] or numerical solutions using a method of stress and velocity characteristics by Sokolovsky [36] for complex cases [37–43]. In turn, in a kinematic approach, different failure mechanisms consisting of slip lines are assumed in the soil. From the equilibrium of forces on sliding wedges, a resultant total earth pressure is calculated [20, 44–47]. A distribution of pressures can only be roughly estimated.

Finite element calculations are more realistic than analytical solutions since they are able to calculate deformations and stresses in each point of the granular material. For FE-analyses, an elasto-plastic [48–52], perfect plastic [53], and hypoplastic [54] law was used. However, a characteristic length was not taken into account.

3. Finite element implementation

The FE-calculations were carried out with a polar hypoplastic law [55–60]. The law can reproduce essential features of granular bodies during shear localisation. It is characterised by simplicity and a wide range of applications. The material constants can be found by means of standard element tests and simple index tests. They are correlated with grain properties. Thus, they can be estimated from granulometric properties (encompassing grain size distribution curve, shape, angularity and hardness of grains) [61, 62]. The capability of this law a has been already demonstrated in solving boundary value problems involving localisation such as biaxial test [55, 60, 63, 64], shearing of a narrow granular layer [11, 59, 65], silo filling [66], silo flow [11, 67], furnace flow [68], footings [56, 69] and sand anchors [70]. A close agreement between calculations and experiments was achieved. The FE-calculations showed also that the thickness of shear zones did not depend upon the mesh discretisation if the size of finite elements in the shear zone was not more than five times the mean grain diameter when using triangular finite elements with linear shape functions for displacements and a Cosserat rotation. Numerical calculations by Sluys [2] and Groen [71] within a polar continuum also indicate that convergence to a unique solution can only be obtained when the element size is small enough compared to the width of the localised zone. For this reason, to realistically model large geotechnical boundary value problems it is necessary to use a Cosserat approach together with a remeshing technique [72].

The FE-analyses of a passive and active earth pressure of a retaining wall for the case of plane strain were carried out with the following material constants

(for so-called Karlsruhe sand): $e_{i0} = 1.3$ (maximum void ratio at pressure equal to zero), $e_{d0} = 0.51$ (minimum void ratio at pressure equal to zero), $e_{c0} = 0.82$ (critical void ratio at pressure equal to zero), $\phi_c = 30°$ (critical angle of internal friction during stationary flow), $h_s = 190$ MPa (granular hardness), $\alpha = 0.3$ (coefficient), $n = 0.5$ (coefficient), $d_{50} = 0.5$ mm (mean grain diameter) and $a_c = a_1^{-1}$ (a_c – micro-polar constant correlated with the grain roughness, a_1 – coefficient determining the shape of the stationary stress surface [73], $a_1^{-1} = 3$–4.5). The parameters h_s and n are determined from a single oedometric compression test with an initially loose specimen [61, 62], h_s reflects the slope of the curve in a semilogarithmic representation, and n its curvature. The constant α is found from a triaxial test with a dense specimen [62]. It reflects the height and position of the peak value of the stress-strain curve. The angle ϕ_c is estimated from the angle of repose or measured in a triaxial test with a loose specimen [62]. The values of e_{i0}, e_{d0}, e_{c0} and d_{50} can be obtained with index tests ($e_{c0} \approx e_{max}$, $e_{d0} \approx e_{min}$, $e_{i0} \approx (1.1$–$1.5)e_{max}$) [73].

The calculations were performed mainly for a sand body with a height of $H = 50$ mm and a length of $L = 100$ mm. Quadrilateral finite elements composed of four diagonally crossed triangles were applied to avoid volumetric locking due to dilatancy effects [71]. Linear shape functions for displacements and the Cosserat rotation were used. Totally, 3200 triangular elements were used. The height and the width of all quadrilateral elements was 2.5 mm ($5 \cdot d_{50}$). Thus, the mesh alignment was $45°$. The height of the retaining wall located at the right side of the sand body was assumed to be $h = 42.5$ mm ($h/H = 0.85$). To examine the influence of the size of the granular specimen and the wall height, the analysis was also carried out with a sand body and a retaining wall being 4 times larger ($H = 200$ mm, $L = 400$ mm, $h = 170$ mm) but with the same quantity of finite elements (3200). The height and the width of quadrilateral elements was then $20 \cdot d_{50}$.

The integration was performed with three sampling points placed in the middle of each element side. The calculations were carried out with large deformations and curvatures (updated Lagrange formulation), changing the element configuration and the element volume. As the initial stress state in the granular specimen, a K_0-state without polar quantities was assumed ($\sigma_{22} = \gamma x_2$, $\sigma_{11} = \sigma_{33} = K_0 \gamma x_2$, $\sigma_{12} = \sigma_{21} = m_1 = m_2 = 0$); σ_{11} – horizontal normal stress, σ_{22} – vertical normal stress, σ_{12} – horizontal shear stress, σ_{21} - vertical shear stress, m_1 – horizontal couple stress, m_2 – vertical couple stress, γ – initial density of sand, x_2 – vertical coordinate measured from the top, $K_0 = 0.40$ – pressure coefficient at rest). Two sides and the bottom of the sand specimen were assumed to be very rough ($u_1 = 0$, $u_2 = 0$, $\omega^c = 0$); u_1 – horizontal displacement, u_2 – vertical displacement, ω^c – Cosserat rotation. The top of the sand specimen was traction and moment free. The retaining wall was assumed to be stiff and very rough ($u_2 = 0$, $\omega^c = 0$). Thus, no slip of sand along the wall was taken into account. Three different wall modes were assumed in passive and active tests: uniform horizontal translation, rotation around the wall bottom and rotation around the wall top. The maximum horizontal displacement increments were chosen as $\Delta u/h = 0.00002$ (passive mode – wall moves away from the backfill) and $\Delta u/h = 0.000004$ (active mode – wall moves against the backfill). About *ca.* 5000 steps were performed.

The calculations were carried out with different initial void ratios of sand: $e_0 = 0.65$, 0.75, 0.85 and 0.95. In addition, the effect of the distribution of e_0 was investigated. In this case, e_0 was distributed stochastically in elements of the sand body by means of a random generator in such a way that the initial void ratio $e_0 = 0.65$ was increased in every element by the value $0.05r$ ($e_0 = 0.65 + 0.05r$), where r is a random number within the range of $(0.01, 0.99)$ [11]. The mean grain diameter of sand was assumed to be constant $d_{50} = 0.5$ mm or distributed stochastically $d_{50} = (0.3 + 0.4r)$ mm.

For the solution of the non-linear equation system, a modified Newton-Raphson scheme with line search was used using an initial global stiffness matrix calculated with only two first terms of the constitutive equations (which are linear in d_{kl}^c and kd_{50}). To accelerate the calculations in the softening regime, the initial increments of displacements and the Cosserat rotation in each calculation step were assumed to be equal to the converged increments from the previous step [10, 11]. In addition, to prevent eventual inadmissible stress states, a substepping algorithm was used (deformation and curvature increments were divided into smaller parts within each step). The iteration steps were performed using translational and rotational convergence criteria. For the time integration of stresses and couple stresses in finite elements, a one-step Euler forward scheme was applied [10, 11].

4. Numerical results

4.1. Passive case

4.1.1. Influence of type of wall movement

The FE-results of a plane strain passive earth pressure problem with a sand body $50\,\text{mm} \times 100\,\text{mm}$ and a retaining wall of a height $h = 42.5\,\text{mm}$ are shown for dense sand ($e_0 = 0.65$, $\gamma = 16.20\,\text{kN/m}^3$) in Figures 1–5. Figure 1 presents the evolution of the normalised horizontal earth pressure force $2E_h/(\gamma h^2)$ versus the normalised horizontal wall displacement u/h for three different wall movements. In the case of a rotating wall, the horizontal displacement u concerns the maximum wall displacement of the bottom point (wall rotating about the top) or of the top point (wall rotating around the bottom). The force E_h was calculated as the integral of mean horizontal normal stresses σ_{11} from quadrilateral elements along the retaining wall. In Figure 2, the deformed meshes with the distribution of the void ratio e in the residual state are shown. The darker region indicates the higher void ratio. The void ratio was taken as the mean value in each quadrilateral element of the mesh. The evolution of the void ratio during the horizontal wall translation is presented in Figure 3. The distribution of the Cosserat rotation ω^c in the residual state for the wall translation is shown in Figure 4. The magnitude of the Cosserat rotation is marked by circles with a maximum diameter corresponding to the maximum rotation in the given step. The distribution of normalised horizontal normal stresses $\sigma_{11}/(\gamma h)$ is presented in Figure 5. The stresses σ_{11} are taken as the mean values from quadrilateral elements at the specimen side.

The curves of horizontal earth pressure $2E_h/(\gamma h^2)$ are similar for the wall translation and wall rotation around the top (Figure 1). The forces increase, reach a maximum for about $u/h = 1\%$, show a pronounced softening then and tend to asymptotic values for about $u/h = 10\%$. For the wall rotation about the bottom, the
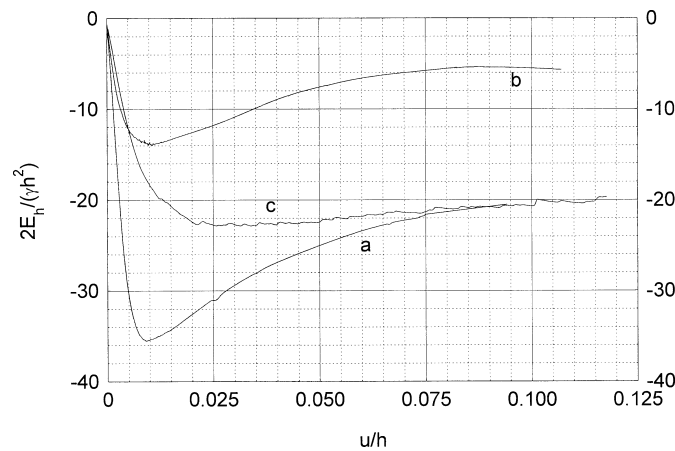
Figure 1. Resultant normalised earth pressure force $2E_h/(\gamma h^2)$ versus normalised wall displacement u/h (passive case, $h = 0.0425$m, dense sand $e_0 = 0.65$): a – translating wall, b – wall rotating around its top, c – wall rotating around its bottom

force increases, reach a peak for $u/h = 2\%$ and then decreases slightly. The maximum force and softening are highest for the wall translation, and the lowest for the wall rotation about the top. The normalised horizontal earth pressure forces are high ($2E_h/\gamma h^2 = 14-36$) due to the high wall roughness and the large relationship between the mean grain diameter and the wall height (shear resistance increases with increasing mean grain diameter and decreasing specimen height [59]). Thus, they are larger than the usual earth pressure coefficients [74] with one circular slip line, $K_{pr} = 11.33-25.80$, and with three plane slip lines, $K_{pt} = 13.40-23.70$, at $\delta = \varphi$ (δ – wall friction angle, $\varphi = 40°-45°$ – internal friction angle of dense sand).

Shear localisation which is characterised among others by the appearance of the Cosserat rotation and a strong increase of the void ratio [59, 60, 63, 64] is strongly dependent on the type of the wall passive mode (Figures 2–4). For the wall translation (Figures 2a and 3), three shear zones are obtained: one horizontal zone appearing at the wall bottom, one nearly circular zone spreading between the wall bottom and the free boundary, and one radial oriented shear zone appearing at the wall top. The circular shear zone becomes dominant in the course of deformation. The horizontal shear zone develops only at the beginning of the wall translation. The radial shear zone forms more slowly than the circular one (it is not fully developed even for $u/h = 10\%$). The material starts to dilate at the same time at three different places (wall bottom, wall top and free boundary), Figure 3a. Next, the inclined dilatant zone (starting from the free boundary) combines with the horizontal dilatant zone (Figure 3b). Later, the radial dilatant zone approaches the inclined zone (Figure 3c). Afterwards, the sand dilatancy takes place mainly along the circular shear zone which is created from the inclined dilatant zone and the horizontal dilatant zone (Figures 3d–f). The thickness of the circular shear zone is about 6mm ($12 \cdot d_{50}$) and its inclination from the bottom is about $\theta = 40°$. The largest void ratio in this zone corresponds approximately to the pressure-dependent critical value $e_c \approx 0.80$. The shear zones can be also detected from the distribution of the Cosserat rotation (Figure 4). The Cosserat rotations are only noticeable in the shear zone [56, 60]. It can been seen (Figure 4) that the radial shear

(a)

(b)

(c)
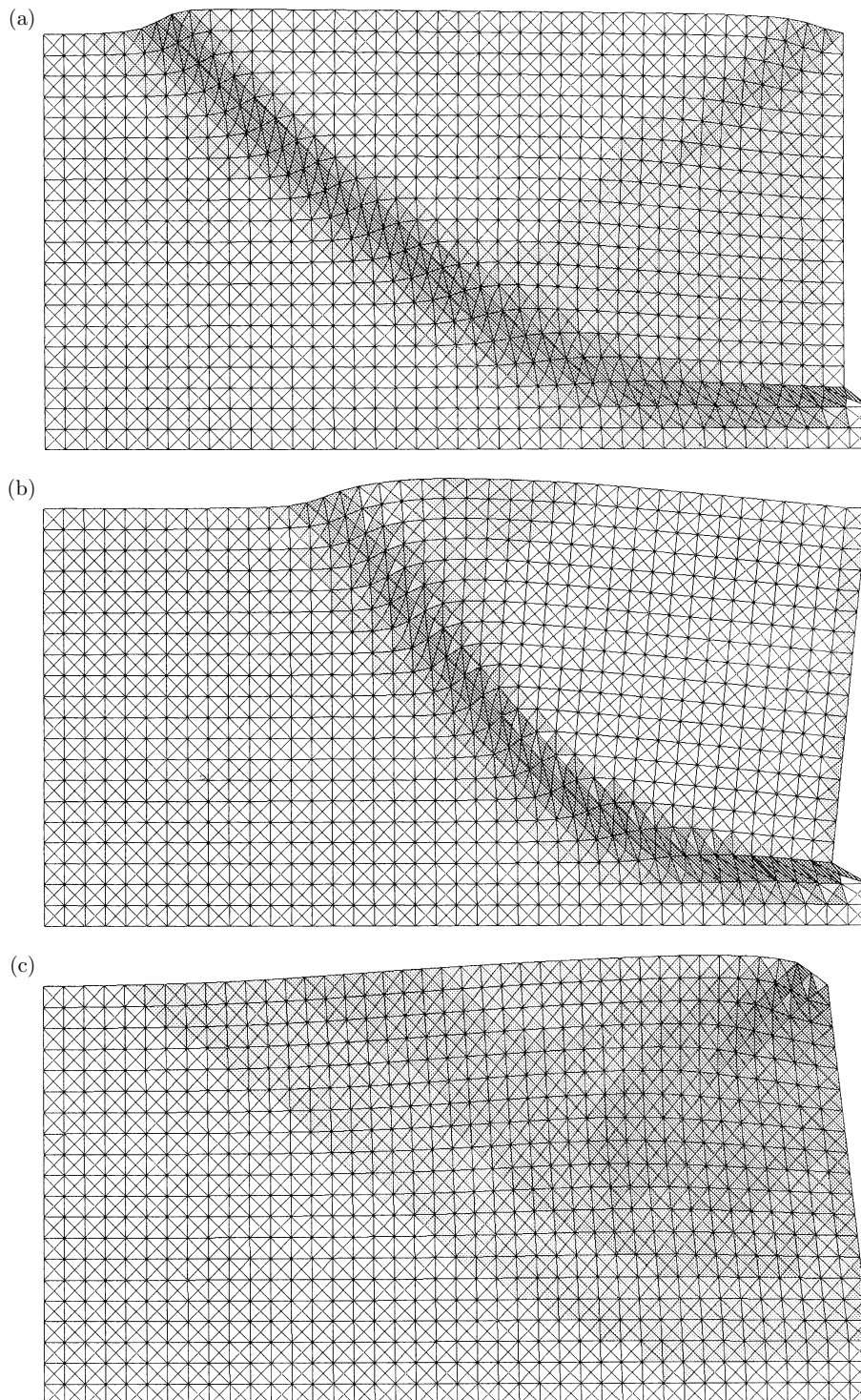
Figure 2. Deformed FE-meshes with distribution of void ratio e for dense sand ($e_0 = 0.65$) during passive earth pressure ($u/h = 0.09$): (a) translating wall, (b) wall rotating around its top, (c) wall rotating around its bottom
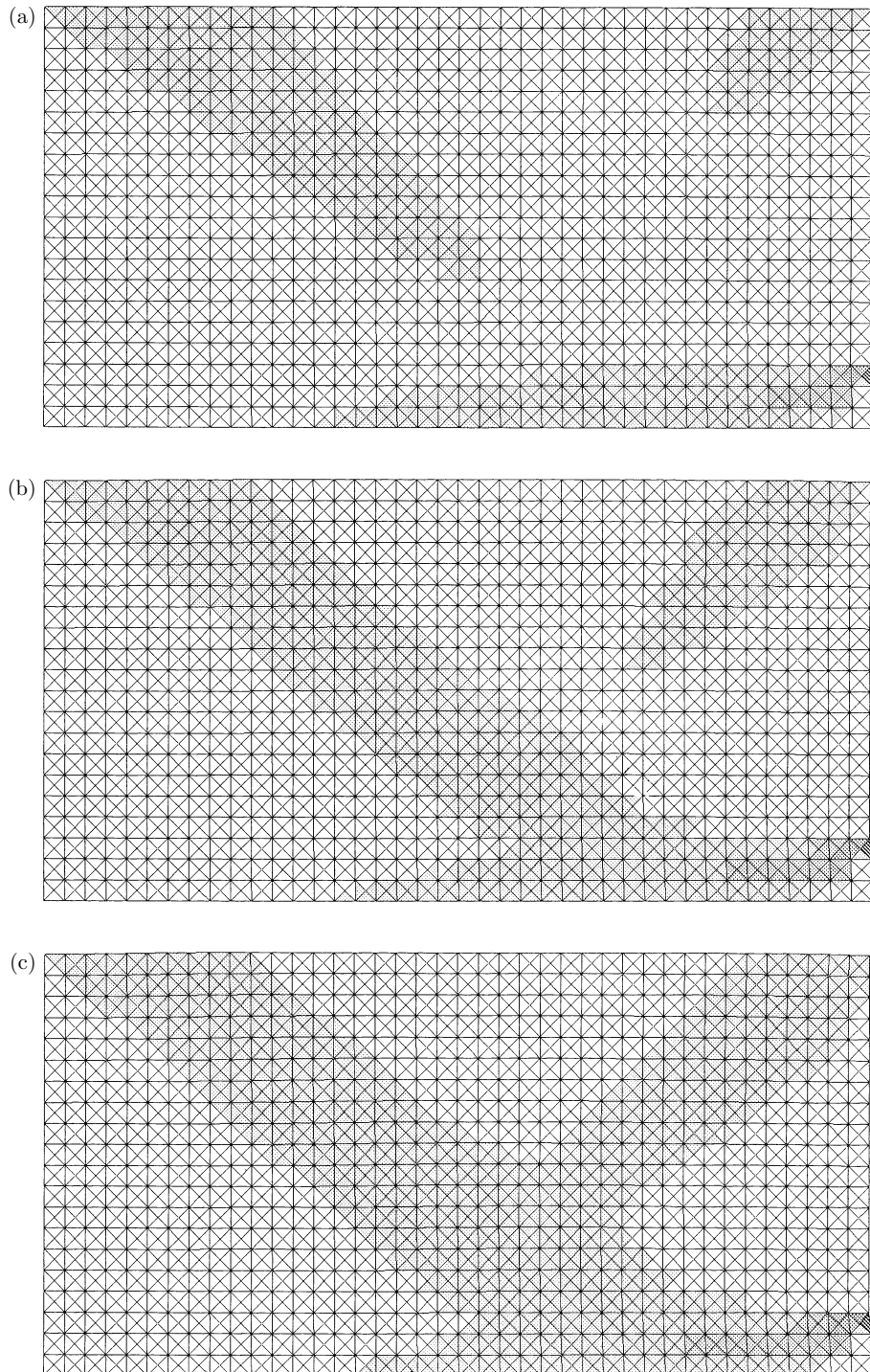
Figure 3. Initial evolution of void ratio e during passive earth pressure with translating wall:
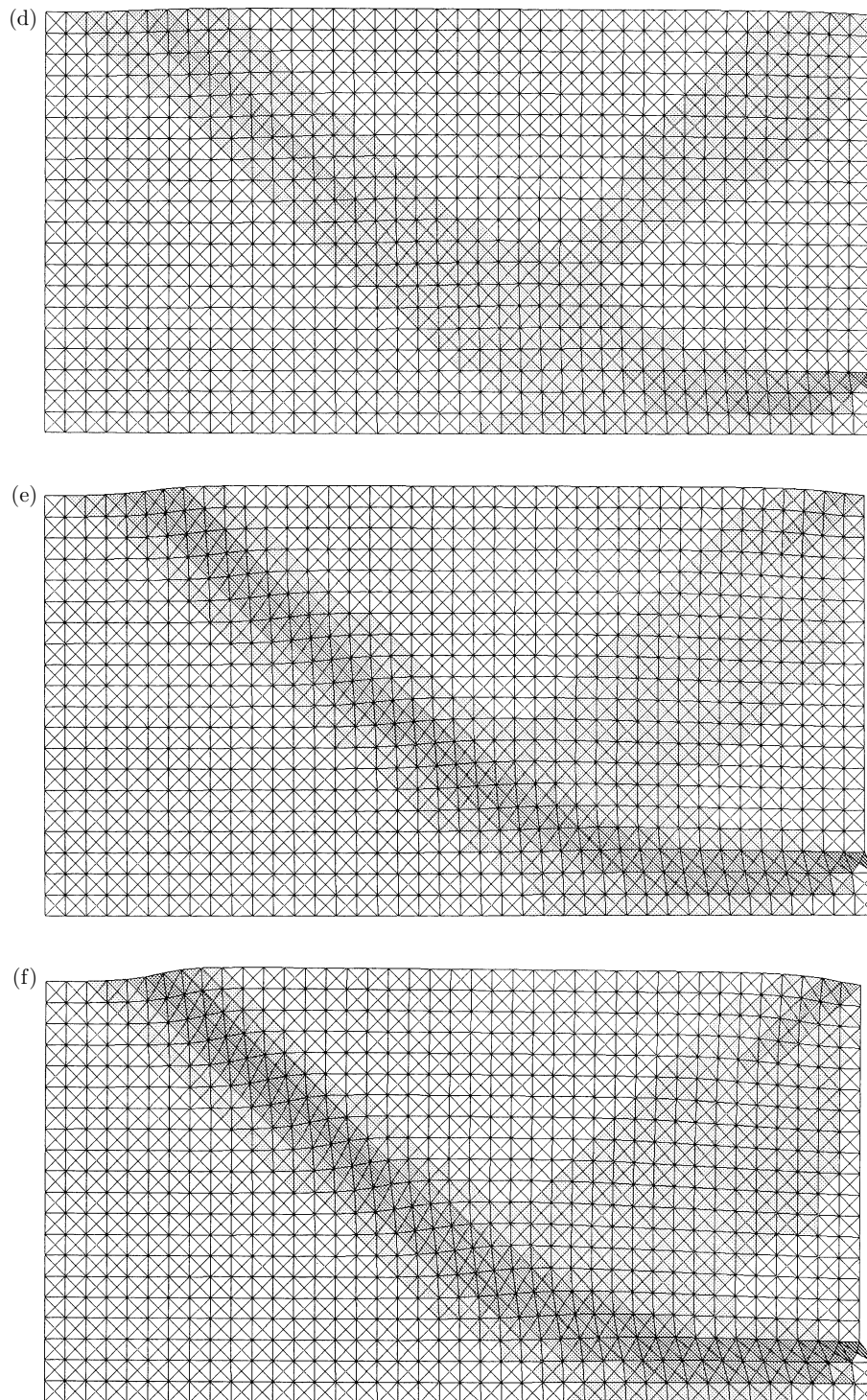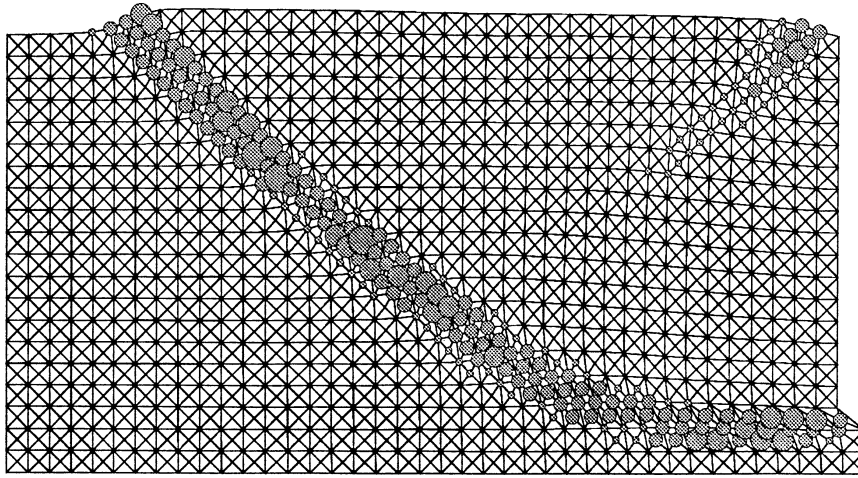(a) $u/h = 0.005$, (b) $u/h = 0.0075$, (c) $u/h = 0.010$

(d)

(e)

(f)

Figure 3 – continued. (d) $u/h = 0.0125$, (e) $u/h = 0.025$, (f) $u/h = 0.05$

Figure 4. Deformed FE-mesh with distribution of Cosserat rotation ω^c for dense sand during
passive earth pressure with translating wall ($e_0 = 0.65$, $u/h = 0.10$)

zone has been not fully developed yet. The geometry of shear zones is in agreement
with experimental observations at the Cambridge University [24] (Figure 6a) and at
the Karlsruhe University [31, 64] (Figure 6b).

In the case of the wall rotation around the top (Figure 2b), only one shear
zone occurs which is more curved than the shear zone during the wall translation.
Its thickness is similar. The calculated deformation field is close to the experimental
one [22, 23] (Figure 7a). When the retaining wall rotates around the bottom (Fig-
ure 2c), only one dilatant shear zone occurs starting at the wall top. It next becomes
diffused. The dilatant region covers the half of the entire granular specimen. It is di-
vided into regions with different density. The sand displacements differ, however, from
the experiments [26] where a pattern of pronounced curved shear zones of a similar
shape was obtained beginning at the wall top (Figure 7b).

The distribution of the horizontal normal stress σ_{11} on the retaining wall is
markedly non-linear and depends strongly on the type of the wall mode (Figure 5).
For the wall translation and wall rotation about the bottom the shape is parabolic
along the entire wall (Figures 5a and 5c). In the case of the wall rotation about the
top (Figure 5b), the normal stress is insignificant in the higher part of the wall. Since
there is a discontinuity at the wall bottom (the case of the wall translation and wall
rotation about the top), a strong jump of stresses is obtained there.

4.1.2. Influence of void ratio

The effect of the initial void ratio on normalised earth pressure force, shear
localisation and horizontal normal stresses along the wall is presented in Figures 8–10
for the case of the horizontal wall translation. The calculations were carried out with
medium dense ($e_0 = 0.75$, $\gamma = 15.2\text{kN/m}^3$), loose ($e_0 = 0.85$, $\gamma = 14.4 \text{ kN/m}^3$) and very
loose sand ($e_0 = 0.95$, $\gamma = 14.0\text{kN/m}^3$).

An increase of the initial void ratio causes a significant decrease of the maximum
passive earth pressure and softening (Figure 8). For loose and very loose sand,

(a)

(b)

(c)
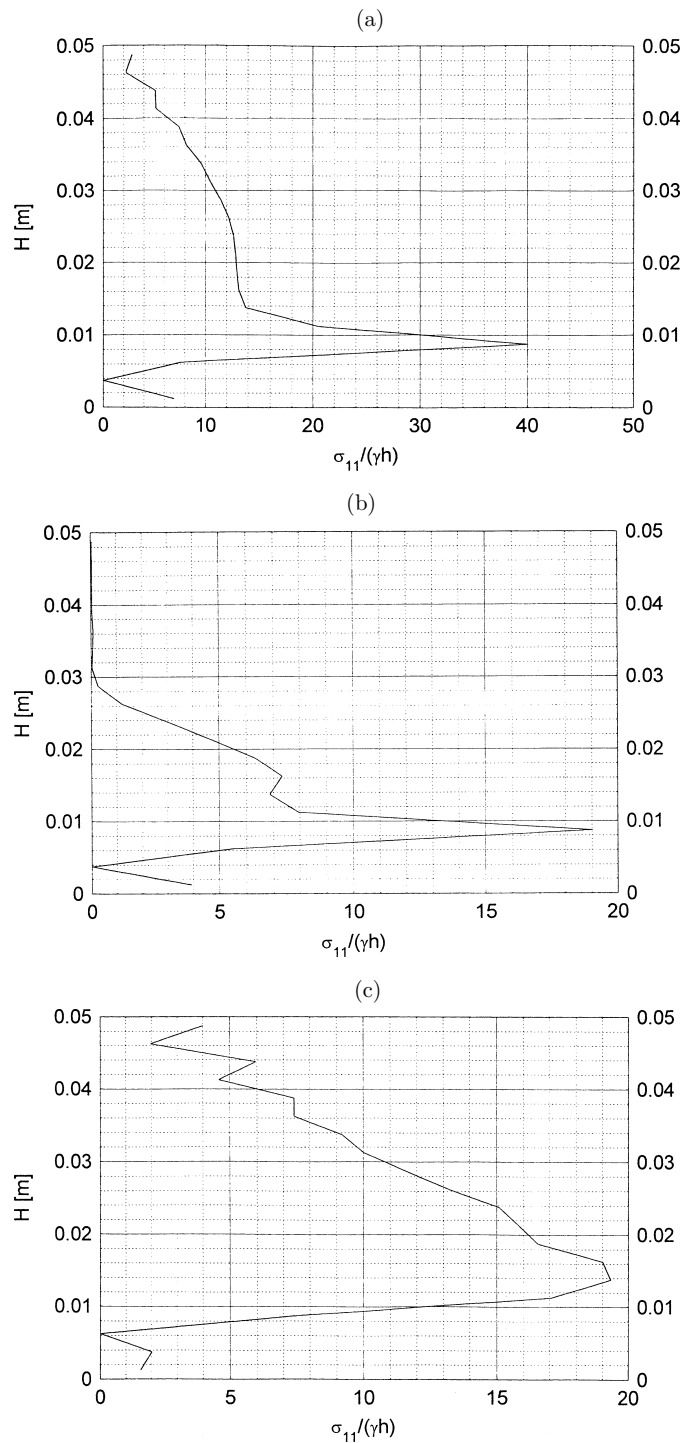
Figure 5. Normalised horizontal normal stresses $\sigma_{11}/(\gamma h)$ along specimen side $H = 0.05$ m during passive earth pressure ($u/h = 0.09$): (a) translating wall, (b) wall rotating around its top, (c) wall rotating around its bottom

(a)

(b)
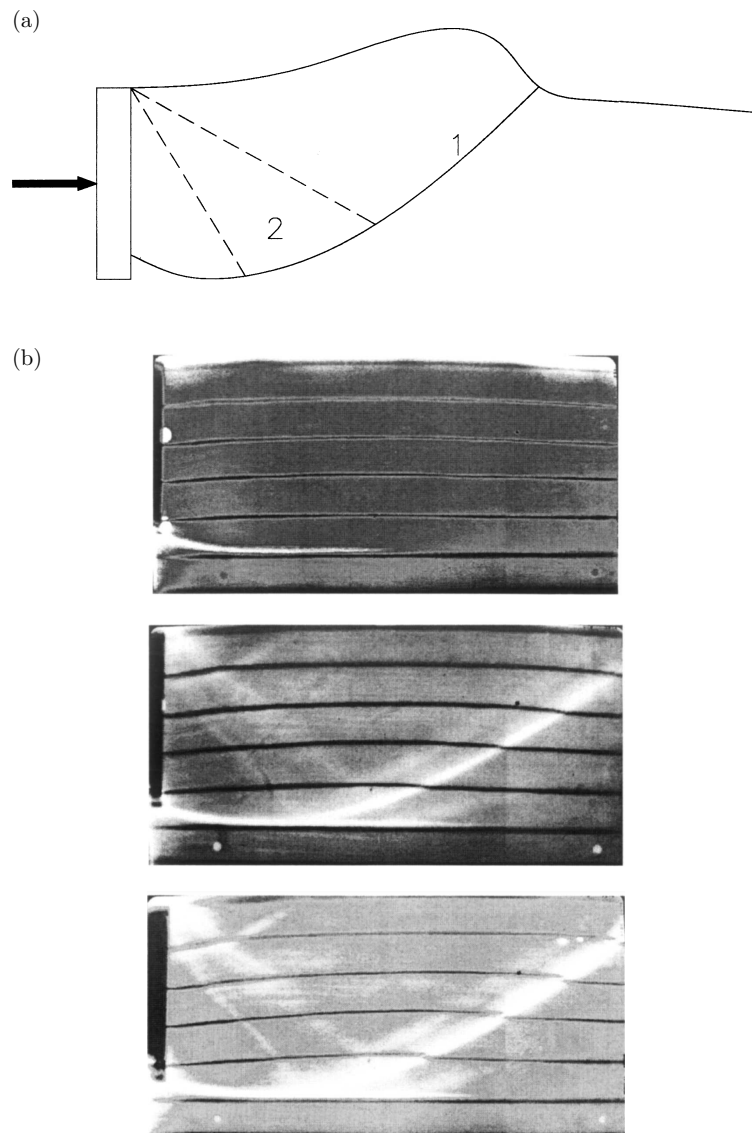
Figure 6. Evolution of shear zone pattern in experiments during a passive horizontal wall
translation: (a) carried out by May [25, 43] and (b) performed by Gudehus [31] and Nübel and
Gudehus [64] (1 – main shear zone, 2 – fan of shear zones)

softening does not take place. The maximum earth pressure force is reached for
$u/h = 0.5\%$.

For medium dense sand, the geometry of shear localisation is similar as in the
case of dense sand since the sand is subject also to dilatancy (Figure 9a). However,
the thickness of the dominant circular shear zone ($t = 8\,\mathrm{mm} = 16 \cdot d_{50}$) and the area
of the diffused dilatant region above the circular shear zone are greater. In the case
of loose sand (Figure 9b), the geometry of shear localisation is also similar. However,
the shear zone behaves contractantly since loose sand due to $e_0 > e_c$ undergoes always
contractancy during shearing. The thickness of the shear zone is also larger. For very
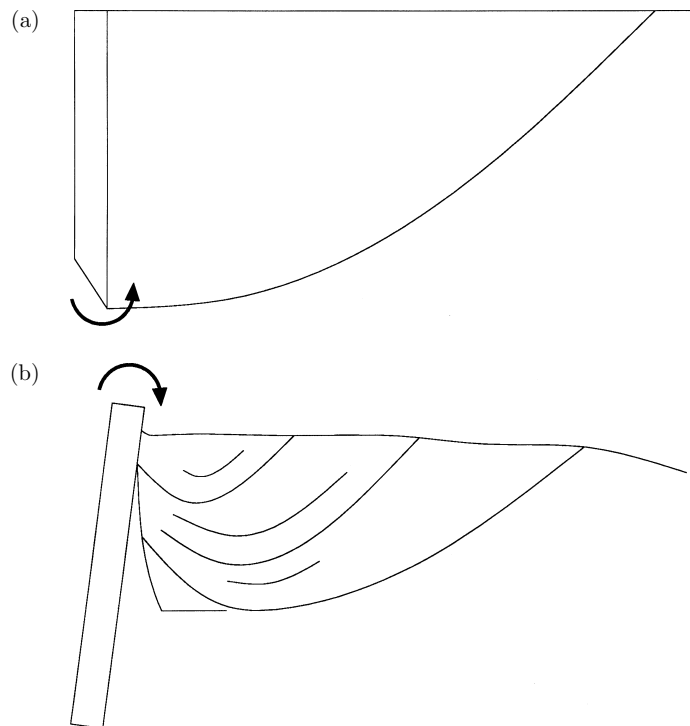
Figure 7. Evolution of shear zone in experiments: (a) during passive wall rotation around the top [23, 43] and (b) during passive wall rotation around the bottom [26, 43]
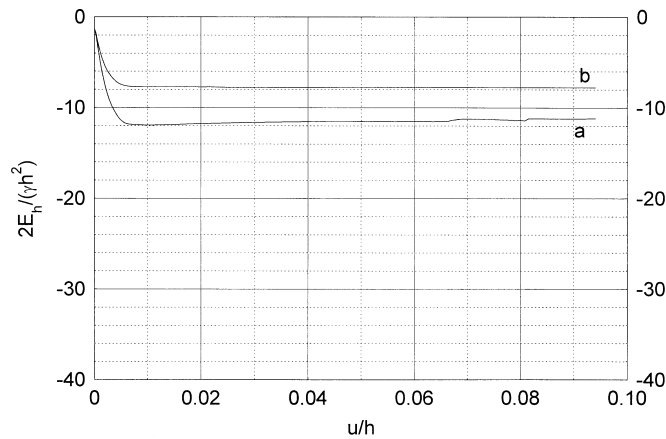

Figure 8. Resultant normalised earth pressure force $2E_h/(\gamma h^2)$ versus normalised wall displacement u/h (translating wall, passive case): a – medium dense sand ($e_0 = 0.75$), b – loose sand ($e_0 = 0.85$)

loose sand (Figure 9c), a clear contractant shear zone appears also along the bottom of the granular specimen.

The distribution of horizontal normal stresses on the wall for medium dense and loose sand is similar as for dense sand except of that a stress jump at the wall bottom does not appear in the case of loose sand (Figure 10).

(a)

(b)

(c)
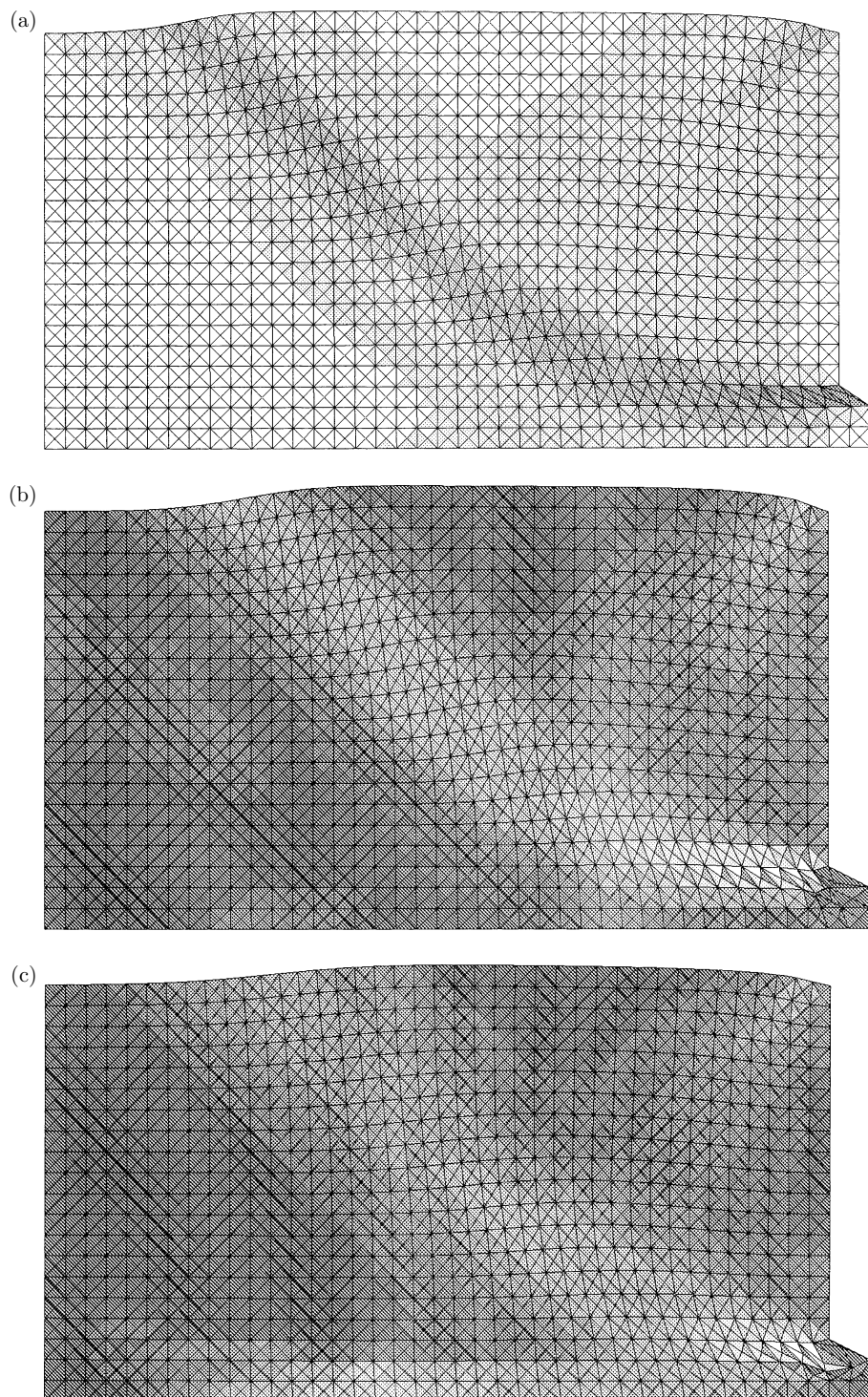
Figure 9. Deformed FE-meshes with distribution of void ratio e for:
(a) medium dense ($e_0 = 0.75$), (b) loose ($e_0 = 0.85$) and (c) very loose sand
($e_0 = 0.95$) during passive earth pressure with translating wall ($u/h = 0.10$)

(a)

(b)
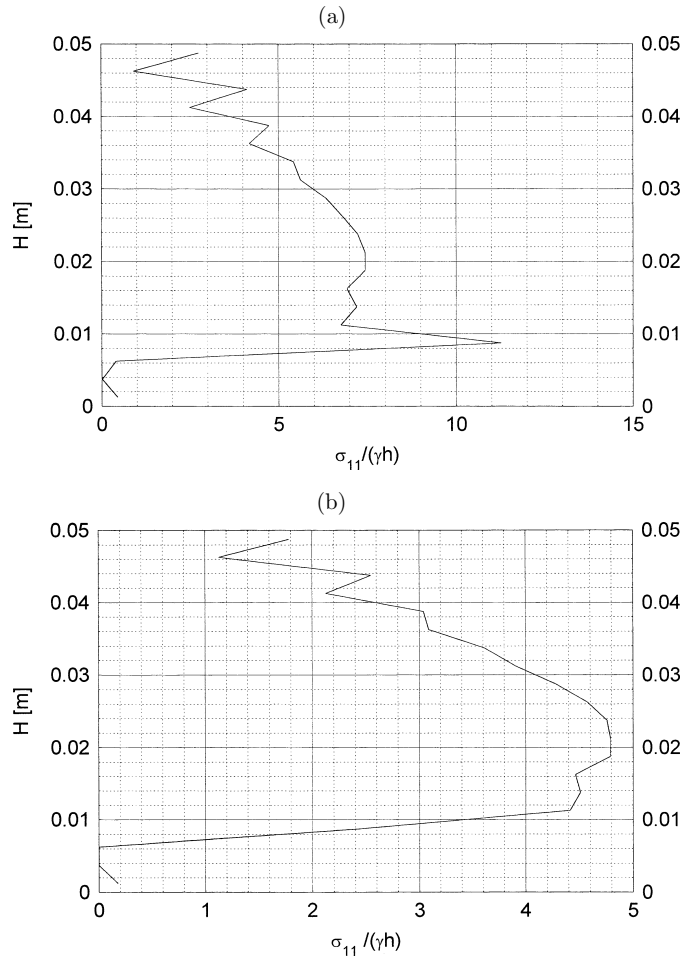
Figure 10. Normalised horizontal normal stresses $\sigma_{11}/(\gamma h)$ along the specimen side $H = 0.05\,\mathrm{m}$
(translating wall, passive case, $u/h = 0.075$): (a) medium dense sand ($e_0 = 0.75$),
(b) loose sand ($e_0 = 0.85$)

4.1.3. Influence of pressure level

The calculations for a horizontally translating wall were performed with a ver-
tical uniform pressure p ($p = 10\mathrm{kPa}$ and $p = 100\mathrm{kPa}$) prescribed to the top boundary
of a dense sand body ($e_0 = 0.65$).

The geometry of shear zones is similar to that of Figure 2a. However, the radial
shear zone moving from the wall top is more pronounced. The thickness of shear zones
is also slightly larger.

4.1.4. Influence of distribution of initial void ratio

The effect of the distribution of the initial void ratio is demonstrated in
Figure 11. The calculations were carried out with a stochastically initially distributed
$e_0 = 0.60 + 0.05r$ (passive wall translation) [11, 60].

The results show that the distribution of the initial void ratio slightly influences
shear zones. The distribution of the void ratio in the shear zone is non-uniform
(Figure 11) and there exist two radial shear zones in contrast to one radial shear
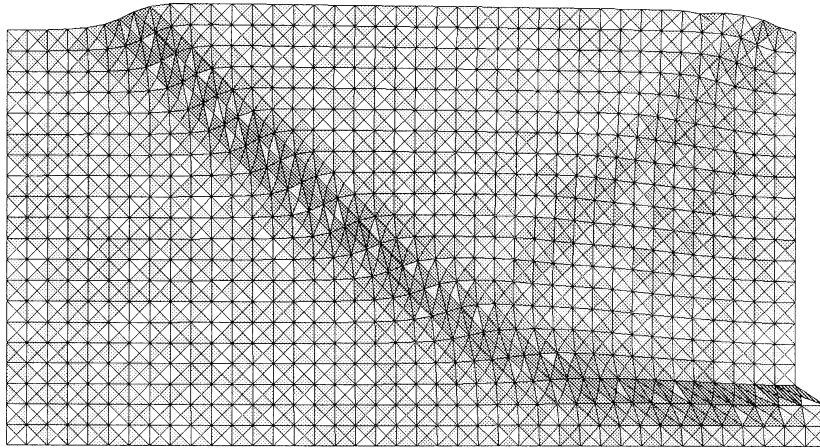
Figure 11. Deformed FE-mesh with distribution of void ratio e for dense sand with stochastic distribution of the initial void ratio ($e_0 = 0.65 + 0.05r$) during passive earth pressure with translating wall ($u/h = 0.08$)
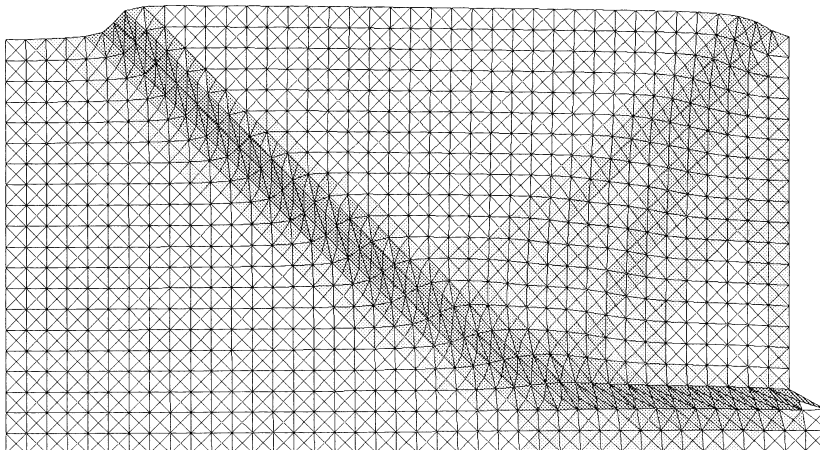
Figure 12. Deformed FE-mesh with distribution of void ratio e for dense sand with stochastic distribution of the mean grain diameter, $d_{50} = (0.3 + 0.4r)\,\text{mm}$, during passive earth pressure with translating wall ($u/h = 0.08$)

zone of Figure 2a. The deformation field is similar to that calculated by Nübel and Gudehus [64]. The maximum normalised horizontal earth pressure force is smaller by 30% due to an increase of the mean initial void ratio.

4.1.5. Influence of distribution of mean grain diameter

Figure 12 presents the deformed mesh with a stochastically distributed mean grain diameter, $d_{50} = 0.3 + 0.4r\,\text{mm}$ [11]. The geometry of shear zones is similar with this of Figure 11. Two radial shear zones moving from the wall top towards the bottom are also obtained.

4.1.6. Influence of specimen size and wall height

Figures 13 and 14 show the results with a larger sand body ($200\,\text{mm} \times 400\,\text{mm}$) and a higher retaining wall ($h = 0.17\,\text{m}$). The maximum normalised horizontal earth
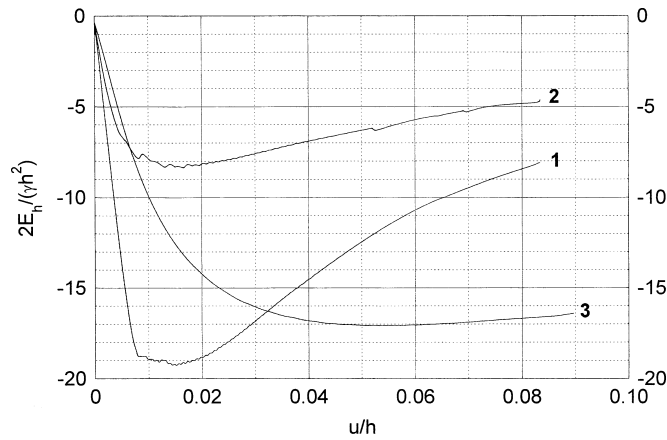
Figure 13. Resultant normalised earth pressure force $2E_h/(\gamma h^2)$ versus normalised wall displacement u/h (passive case, $h = 0.17$m, dense sand $e_0 = 0.65$): 1 – translating wall, 2 – wall rotating around its top, 3 – wall rotating around its bottom

pressure forces, $2E_h/(\gamma h^2) = 9 - 20$, are twice as small as for a smaller sand specimen of 50×100 mm^2. They occur slightly later due to an increase of the pressure level ($u/h = 1.5\% - 5\%$). The evolution of forces (Figure 13) is similar to the one of Figure 2. However, the residual force for the wall rotating along the bottom is higher now than the one for the wall translating horizontally.

In the case of the wall rotation around the top and around the bottom (Figures 14b and 14c), the geometry of shear zones is similar as for a smaller sand specimen. However, for the wall translation (Figure 14a), one radial shear zone appearing at the wall top is both more pronounced and developed. It is connected to the circular shear zone. The thickness of the nearly circular shear zone is about twice larger ($24 \cdot d_{50}$). To get a more exact thickness of the shear zone, the mesh in the region of their occurrence should be refined. The inclination of the shear zone is similar as in Figure 2a.
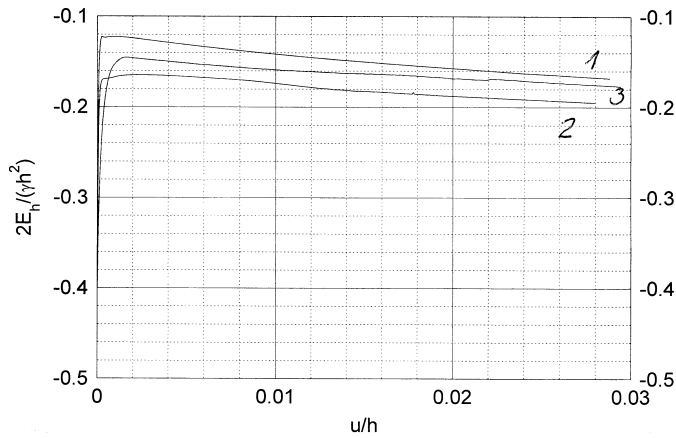
4.2. Active case

The FE-results of a plane strain active earth pressure problem with a sand specimen of 50×100 mm^2 and a retaining wall of $h = 0.0425$ m are shown in Figures 15–17. Figure 15 shows the evolution of the normalised horizontal earth pressure force $2E_h/(\gamma h^2)$ versus the normalised horizontal wall displacement u/h for three different wall thrusts in the case of dense sand ($e_0 = 0.65$, $\gamma = 16.20$ kN/m^3). In Figure 16, the deformed meshes with the distribution of the void ratio in the residual state are shown. The distribution of normalised horizontal normal stresses $\sigma_{11}/\gamma h$ along the entire side of the granular specimen with the retaining wall is presented in Figure 17.

All earth pressure curves drop sharply at the beginning of the wall movement, reach the minimum at $u/h = 0.1\%$ and next increase continuously (Figure 15). Their increase is insignificant. The residual state was not reached for $u/h = 3\%$. The lowest earth pressure force occurs with the wall translation, and the largest with the wall rotation about the top. Thus, the relationship between the earth pressure and the type of the wall movement is inversed as compared to passive earth pressure. The minimum normalised earth pressure forces ($2E_h/(\gamma h^2) = 0.12–0.17$) are approximately equal the

(a)

(b)

(c)
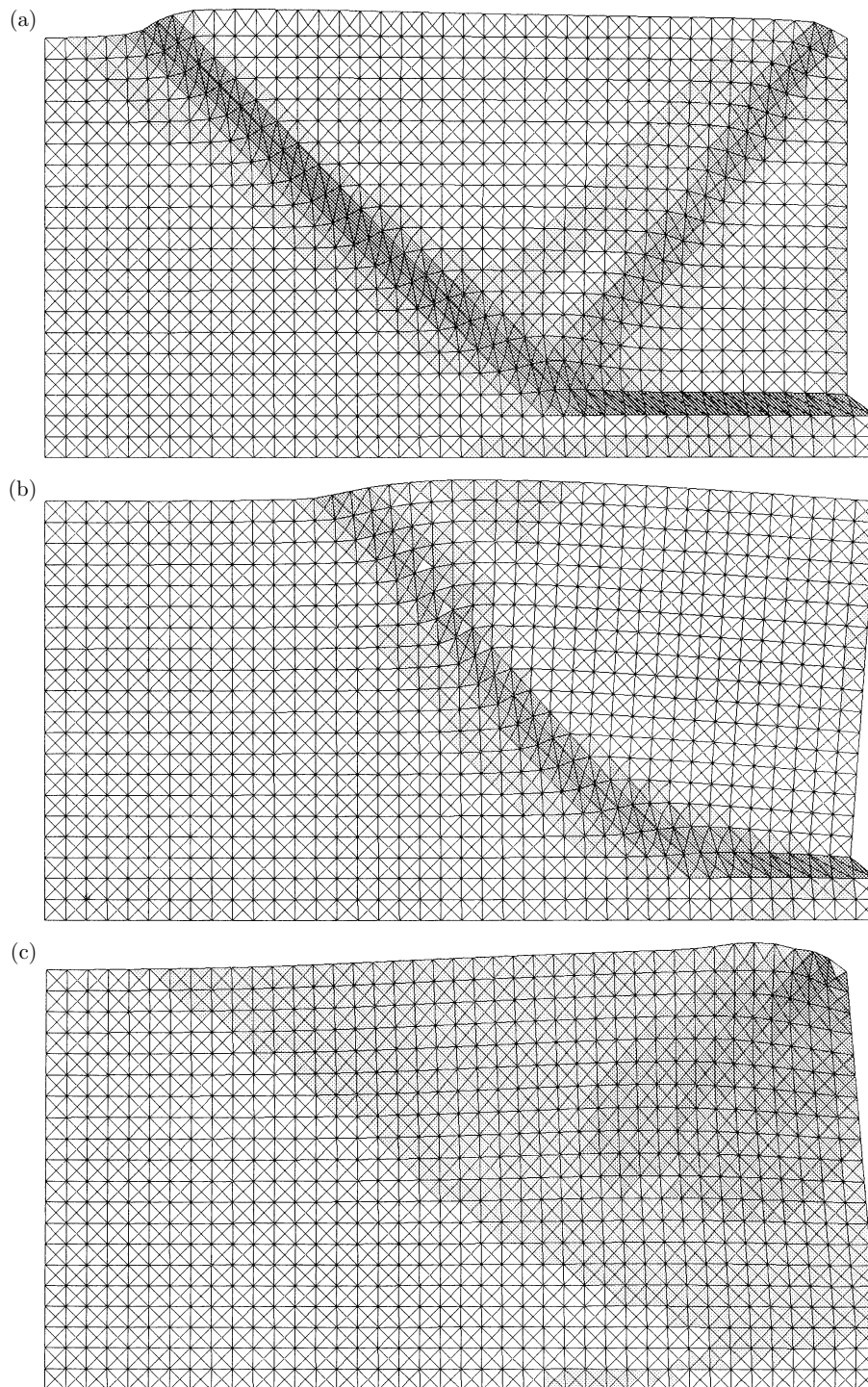
Figure 14. Deformed FE-meshes with distribution of void ratio e for dense sand ($e_0 = 0.65$) during passive earth pressure ($u/h = 0.08$, $h = 0.17$ m): (a) translating wall, (b) wall rotating around its top, (c) wall rotating around its bottom

Figure 15. Resultant normalised earth pressure force $2E_h/(\gamma h^2)$ versus normalised wall displacement u/h (active case, $h = 0.0425\,\mathrm{m}$, dense sand $e_0 = 0.65$): 1 – translating wall, 2 – wall rotating around its top, 3 – wall rotating around its bottom

earth pressure coefficients [74] with a circular slip line, $K_a = 0.157$–0.195 or a plane slip line, $K_a = 0.14$–0.16, with $\delta = \varphi$ ($\varphi = 40°$–$45°$).

The geometry of shear zones depends on the type of the wall movement. In the case of the wall translation, two pronounced shear zones are obtained (Figure 16a). A vertical one occurs along the wall, and the second one propagates from the wall bottom up to the free boundary. The shear zone is slightly curved with a mean inclination to the bottom of $\theta = 50°$. The thickness of the shear zone is about $8.5 \cdot d_{50}$. When the wall rotates around the top, two (not fully developed) shear zones are obtained: the first along the wall and the second inside of sand starting from the wall bottom (Figure 16b). They become slightly diffused in the upper region of the specimen. With a wall rotating about the bottom, only one pronounced shear zone along the wall appears (Figure 16c). Behind the wall, the entire granular material behaves dilatantly. Compared to the experimental observations, similar shear zones were obtained for the wall translation [39] and wall rotation around the top [28]. However, significant differences occur in the case of the wall rotation around the bottom [29] where a pattern of three almost straight shear zones was observed (Figure 18).

The horizontal normal stresses on the wall are non-linear (Figure 17).

5. Conclusions

The following conclusions can be drawn on the basis of the performed FE-studies on shear localisation during plane strain earth pressure problems with very rough and rigid retaining walls:

- The geometry of shear zones depends mainly on the direction and the type of the wall movement (passive or active, translation or rotation). For the passive wall translation, it depends slightly also on the specimen size. The calculated deformation field is qualitatively in agreement with experimental results except of the cases with a rotating wall around the bottom.

J. Tejchman
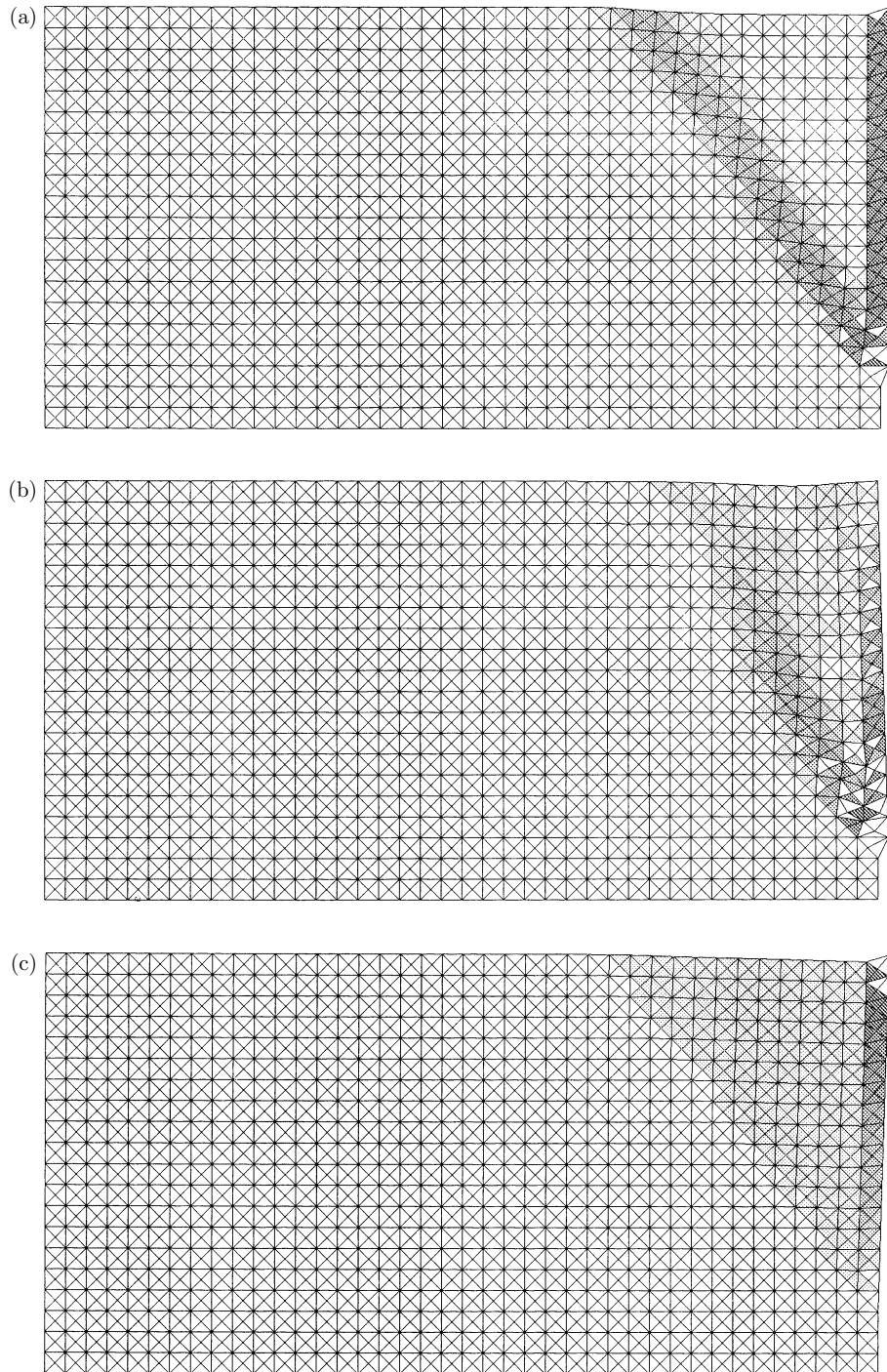
Figure 16. Deformed FE-meshes with distribution of void ratio e for dense sand ($e_0 = 0.65$) during active earth pressure ($u/h = 0.025$): (a) translating wall, (b) wall rotating around its top, (c) wall rotating around its bottom

(a)

(b)

(c)
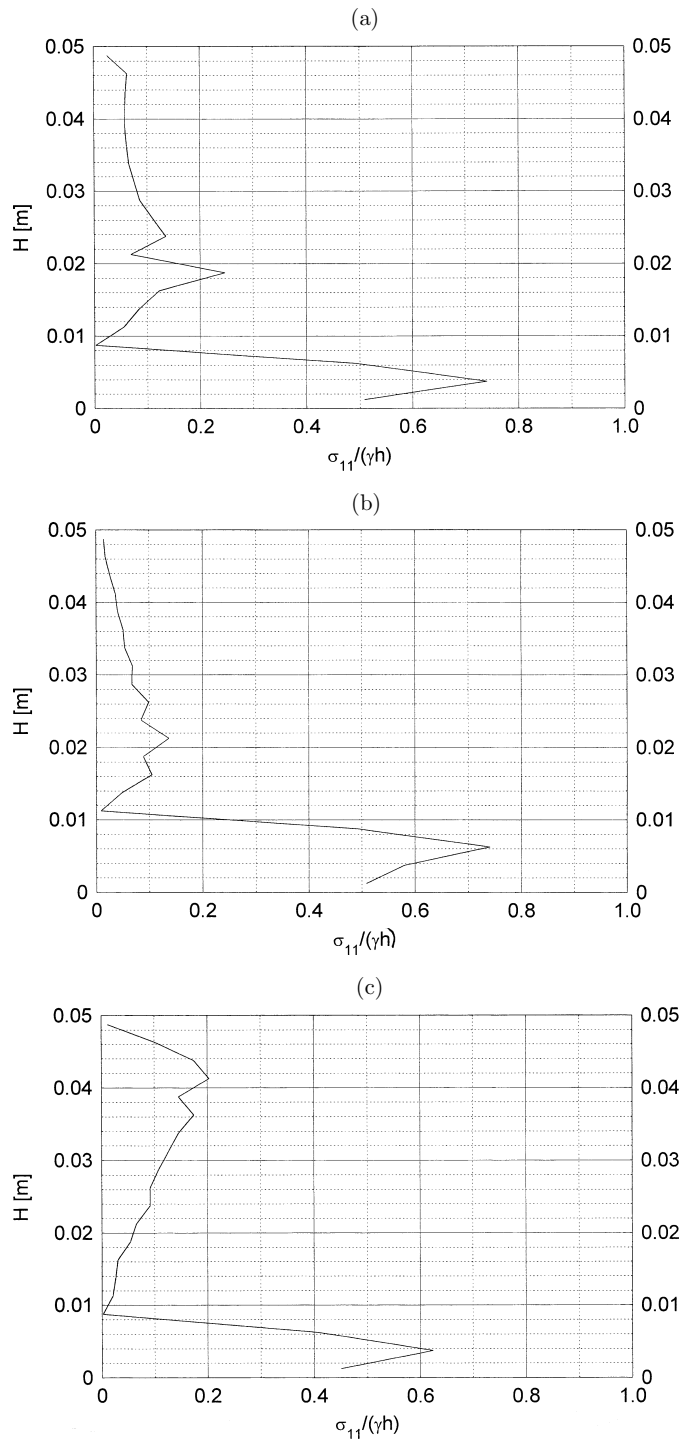
Figure 17. Normalised horizontal normal stresses $\sigma_{11}/(\gamma h)$ along specimen side $H = 0.05\,\mathrm{m}$ during active earth pressure ($u/h = 0.025$): (a) translating wall, (b) wall rotating around its top, (c) wall rotating around its bottom
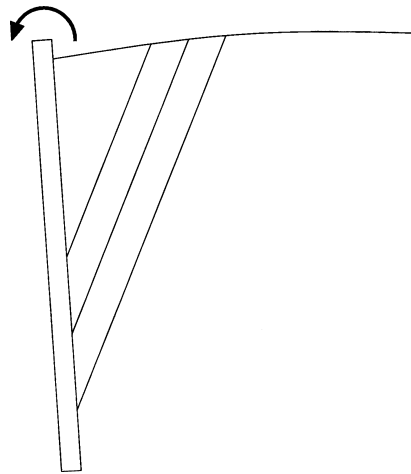
Figure 18. Evolution of shear zone pattern in experiments during passive wall rotation
about the bottom [29, 43]

- The effect of an initial stochastic distribution of void ratio and mean grain diameter on the geometry of shear zones is rather small.
- The largest passive earth pressures occur with the horizontal translation of the wall, they are smaller with the wall rotation around the bottom and again smaller with the wall rotation around the top. In the case of active earth pressure, the largest earth pressures occur during the wall rotation around the top, and the smallest ones during the horizontal wall translation.
- Earth pressure coefficients from model tests (passive case) cannot be directly transferred to large retaining walls due to a scale effect caused by the pressure level and mean grain diameter related to the specimen size.
- The distribution of pressures along the wall is non-linear.
- The thickness of shear zones increases with increasing initial void ratio and pressure level.
- The polar quantities become noticeable by shearing. The Cosserat rotation, the increasing void ratio and the non-symmetry of the stress tensor in the shear zone, and high gradients of curvatures, stresses and couple stresses at the shear zone edges can be used to identify shear zones.

The FE-calculations on the evolution of shear zones during passive and active earth pressure will be continued. The effect of the wall roughness, wall stiffness and wall anchors will be analysed. The FE-results will be directly compared with experimental findings.

References

[1] Aifantis E C 1984 *J. Eng. Mater. Technol.* **106** 326
[2] Sluys L J 1992 *Wave Propagation, Localisation and Dispersion in Softening Solids*, PhD Thesis, Delft University of Technology
[3] de Borst R, Mühlhaus H B, Pamin J and Sluys L Y 1992 *Proc. 3rd Int. Conf. Comp. Plasticity*, (Owen D R J, Onate E and Hinton E, Eds.), Pineridge Press, Swansea, pp. 483–508
[4] Pamin J 1994 *Gradient-dependent Plasticity in Numerical Simulation of Localisation Phenomena*, PhD Thesis, Delft University

[5] Loret B and Prevost J H 1991 *ASCE J. Engng. Mech.* **117** 907

[6] Bazant Z and Lin F B 1988 *Int. J. Num. Meth. Eng.* **26** 1805

[7] Brinkgreve R 1994 *Geomaterial Models and Numerical Analysis of Softening*, PhD Thesis, Delft University

[8] Mühlhaus H B 1989 *Ing. Arch.* **59** 124

[9] Mühlhaus H B 1990 *Comprehensive Rock Engineering* **2** 209

[10] Tejchman J 1989 *Publication Series of the Institute of Soil and Rock Mechanics, University Karlsruhe* **117** 1

[11] Tejchman J 1997 *Publication Series of the Institute of Soil and Rock Mechanics, University Karlsruhe* **140** 1

[12] de Borst R 1991 *Engng. Comput.* **8** 317

[13] Steinmann P 1995 *Int. J. Num. Meth. Engng.* **38** 583

[14] Tejchman J 1995 *Numerical Models in Geomechanics* (Pande G N and Pietruszczak S, Eds.), NUMOG, Davos, pp. 571–576

[15] Vardoulakis I 1980 *Int. J. Num. Anal. Meth. Geomech.* **4** 103

[16] Tatsuoka F, Okahara M, Tanaka T, Tani K, Morimoto T and Siddiquee M S 1991 *Proc. of the ASCE Geotechnical Engineering Congress* **27** (2) 788

[17] Tatsuoka F, Siddiquee M S, Yoshida T, Park C S, Kamegai Y, Goto S and Kohata Y 1994 *Testing Methods and Results of Element Tests and Testing Conditions of Plane Strain Model Bearing Capacity Tests Using Air-dried Dense Silver Buzzard Sand*, Internal Report, University of Tokyo, pp. 1–129

[18] Tatsuoka F, Goto S, Tanaka T, Tani K and Kimura Y 1997 *Deformation and Progressive Failure in Geomechanics* (Asaoka A, Adachi T and Oka F, Eds.), Pergamon, pp. 133–139

[19] Desrues J and Hammad W 1989 *Lecture at Int. Workshop on Numerical Methods for Localization and Bifurcation of Granular Bodies*, Gdansk, Poland

[20] Coulomb C A 1775 *Essai sur une application*, Ed. Science et Industrie, Paris

[21] Darwin G H 1883 *Proc. Inst. Civ. Eng.* **71** 350

[22] Arthur J R F 1962 *Strains and Lateral Force in Sand*, PhD Thesis, University of Cambridge

[23] James R G 1965 *Stress and Strain Fields in Sand*, PhD Thesis, University of Cambridge

[24] Lucia J B A 1966 *Passive Earth Pressure and Failure in Sand*, Research Report, University of Cambridge

[25] May J 1967 *A Pilot Project on the Cutting of Soils*, Research Report, University of Cambridge

[26] Bransby P L 1968 *Stress and Strain in Sand Caused by Rotation of a Model Wall*, PhD Thesis, University of Cambridge

[27] Adeosun A 1968 *Lateral Forces and Failure Patterns in the Cutting of Sands*, Research Project, University of Cambridge

[28] Lord J A 1969 *Stress and Strains in an Earth Pressure Problem*, PhD Thesis, University of Cambridge

[29] Smith I 1972 *Stress and Strain in a Sand Mass Adjacent to a Model Wall*, PhD Thesis, University of Cambridge

[30] Milligan G W E 1974 *Geotechique* **26** (3) 473

[31] Gudehus G 1986 *Felsbau* **4** 190

[32] Schwing E 1991 *Publication Series of the Institute of Soil and Rock Mechanics, University Karlsruhe* **121** 1

[33] Dembicki E 1979 *Passive, Active Earth Pressure and Bearing Capacity of Soil*, Arkady, Warsaw (in Polish)

[34] Caquot A and Kerisel J 1948 *Tables for the Calculation of Passive Pressures, Active Pressures and Bearing Capacity of Foundations*, Gauthier-Villars, Paris

[35] Negre R 1959 *Sur une Methode Approchee de la Repatition des Equilibre Limite des Massifs Plans a Faible Frottement Interne*, C. R. A. S., Paris, pp. 3118–3120

[36] Sokolovski V V 1965 *Statics of Granular Media*, Pergamon Press

[37] Roscoe K H 1970 *Geotechnique* **20** (2) 129

[38] James R G and Bransby P L 1971 *Geotechnique* **21** (1) 61

[39] Szczepiński W 1974 *Limit States and Kinematics of Granular Materials*, PWN, Warsaw (in Polish)

[40] Bransby P L and Milligan G W E 1975 *Geotechnique* **25** (2) 175

[41] Houlsby G T and Wroth C P 1982 *Proc. 4th Int. Conf. on Num. Meth. in Geomech.*, Edmonton, Canada, pp. 1059–1071

[42] Milligan G W E 1983 *Geotechnique* **33** (1) 41

[43] Leśniewska D 2000 *Analysis of Shear Band Pattern Formation in Soil*, DSc Thesis, Institute of Hydroengineering of the Polish Academy of Sciences, Gdansk, Poland

[44] Terzaghi K 1951 *Mecanique Theorique des Sols*, Dunod., Paris

[45] Gudehus G 1978 *Advances in Analysis of Geotechnical Instabilities* **13** 1

[46] Wang Y Z 2000 *Geotechnique* **50** (1) 83

[47] Leśniewska D and Mróz Z 2000 *Geotechnique* (in print)

[48] Simpson B 1972 *The Uses of Finite Element Technique in Soil Mechanics with Particular Reference to Deformation in Plane Strain*, PhD Thesis, University of Cambridge

[49] Simpson B and Wroth C P 1974, 1982 *Proc. Int. Conf. on Num. Meth. in Geomech.* (Eisenstein Z, Ed.), Edmonton, pp. 85–93

[50] Christian J T, Hagmann A J and Marr W A 1977 *Int. J. Num. Anal. Meth. Geomech.* **1** 343

[51] Potts D M and Fourie A B 1984 *Geotechnoque* **34** (3) 383

[52] Fourie A B and Potts D M 1989 *Geotechnique* **39** (2) 175

[53] Nakai T 1985 *Proc. Int. Conf. Num. Meth. Geomech.*, Nagoya, pp. 765–772

[54] Ziegler M 1986 *Berechnung des verschiebungsabhängigen Erddruckes in Sand*, PhD Thesis, Institute for Soil and Rock Mechanics, Karlsruhe University

[55] Tejchman J, Herle I and Wehr J 1999 *Int. J. Num. Anal. Meth. Geomech.* **23** 2045

[56] Tejchman J and Herle I 1999 *Soils and Foundations* **39** (5) 47

[57] Tejchman J 2000 *Granular Matter* **2** (2) 77

[58] Tejchman J and Ummenhofer T 2000 *Thin-Walled Structures* **37** 333

[59] Tejchman J and Gudehus G 2001 *J. Num. and Anal. Methods in Geomechanics* **23** 2045

[60] Tejchman J 2001 *Acta Mechanica* (in print)

[61] Herle I 1998 *Localisation and Bifurcation Theory for Soils and Rocks in Gifu* (Adachi T, Oka F and Yashima A, Eds.), Balkema, pp. 91–99

[62] Herle I and Gudehus G 1999 *Mechanics of Cohesive-Frictional Materials* **4** (5) 461

[63] Tejchman J and Bauer E 1996 *Computers and Geotechnics* **19** (3) 221

[64] Nübel K and Gudehus G 2001 *Powder and Grains* (in print)

[65] Bauer E and Huang W 1999 *Numerical Models in Geomechanics* (Pande G N, Pietruszczak S and Schweiger H F, Eds.), Balkema, pp. 133–141

[66] Tejchman J 1998 *Powder Technology* **96** 227

[67] Tejchman J and Gudehus G 1993 *Powder Technology* **76** (2) 201

[68] Zaimi S A 1998 *Modelisation de l'Coulement des Charges dans le Haut Fourneau*, PhD Thesis, Ecole Centrale, Paris, France

[69] Maier P 2000 *Numerical Calculations of Foundations on Sand*, Internal Report of the Institute for Soil Mechanics, University of Dortmund, Germany

[70] Wehr J and Tejchman J 1999 *Proc. World Civil and Environmental Engineering Conference* (Balasubramaniam A S et al., Eds.), Thailand

[71] Groen A E 1997 *Three-dimensional Elasto-plastic Analysis of Soils*, PhD Thesis, Delft University

[72] Ehlers W and Volk W 1997 *Mechanics of Cohesive-Frictional Materials* **2** 301

[73] Bauer E 2000 *Mechanics of Cohesive-Frictional Materials* **5** 125

[74] Gudehus G 1996 *Erddruckermittlung*, Grundbautaschenbuch, Teil 1, Ernst und Sohn